JGR Atmospheres

RESEARCH ARTICLE
10.1029/2023JD039354

Negative Excursion of Surface Electric Fields During Gamma-Ray Glows in Winter Thunderstorms

Y. Wada[1], M. Kamogawa[2], M. Kubo[3], T. Enoto[4,5], S. Hayashi[6], T. Sawano[7], D. Yonetoku[8], and H. Tsuchiya[9]

[1]Division of Electrical, Electronic and Infocommunications Engineering, Graduate School of Engineering, Osaka University, Osaka, Japan, [2]Natural Disaster Research Section, Global Center for Asian and Regional Research, University of Shizuoka, Shizuoka, Japan, [3]Faculty of Frontier Engineering, Institute of Science and Engineering, Kanazawa University, Kanazawa, Japan, [4]Department of Physics, Graduate School of Science, Kyoto University, Kyoto, Japan, [5]Extreme Natural Phenomena RIKEN Hakubi Research Team, Cluster for Pioneering Research, RIKEN, Saitama, Japan, [6]Meteorological Research Institute, Japan Meteorological Agency, Tsukuba, Japan, [7]Advanced Research Center for Space Science and Technology, Institute of Science and Engineering, Kanazawa University, Kanazawa, Japan, [8]School of Mathematics and Physics, College of Science and Engineering, Kanazawa University, Kanazawa, Japan, [9]Nuclear Science and Engineering Center, Japan Atomic Energy Agency, Ibaraki, Japan

Key Points:

- In the 2020–2021 winter season, 6 gamma-ray glows were detected at Kanazawa University, Japan, with electric-field measurement
- Surface electric fields were negative during the detection of all the gamma-ray glows
- High-energy electrons seemed to be produced between a well-developed negative charge region and a localized positive charge region below

Correspondence to:
Y. Wada,
wada@yuuki-wd.space

Citation:
Wada, Y., Kamogawa, M., Kubo, M., Enoto, T., Hayashi, S., Sawano, T., et al. (2023). Negative excursion of surface electric fields during gamma-ray glows in winter thunderstorms. *Journal of Geophysical Research: Atmospheres*, *128*, e2023JD039354. https://doi.org/10.1029/2023JD039354

Received 1 JUN 2023
Accepted 19 OCT 2023

Author Contributions:

Conceptualization: Y. Wada, M. Kamogawa
Data curation: Y. Wada, M. Kamogawa, M. Kubo, S. Hayashi
Formal analysis: Y. Wada
Funding acquisition: Y. Wada, T. Enoto, H. Tsuchiya
Investigation: Y. Wada, M. Kamogawa, S. Hayashi, T. Sawano, D. Yonetoku, H. Tsuchiya
Methodology: Y. Wada, M. Kamogawa
Project Administration: Y. Wada, T. Enoto, H. Tsuchiya
Resources: Y. Wada, M. Kamogawa, M. Kubo, S. Hayashi, T. Sawano, D. Yonetoku
Software: Y. Wada
Supervision: Y. Wada
Validation: Y. Wada
Visualization: Y. Wada
Writing – original draft: Y. Wada
Writing – review & editing: M. Kamogawa, T. Enoto, S. Hayashi, H. Tsuchiya

Abstract During the 2020–2021 winter season, we detected 6 gamma-ray glows at Kanazawa University, Japan. Negative surface electric fields (E-fields; in the sign convention of atmospheric electricity) were observed by a field mill during all the glow cases. In five of the six cases, the peak E-field reached around -12 kV m^{-1}, and the E-field during the glow detection was the strongest in the interval including 3 hr before and after the detection time. Therefore, negative charges should have been dominant in the thunderclouds that produced the gamma-ray glows, and electrons were probably accelerated and multiplied by the E-fields between a predominantly negative charge layer and a localized positive charge layer below. In addition, we extracted 8 non-detection cases in the 2020–2021 winter season, in which surface E-fields were stronger than -12 kV m^{-1}. In 5 of the 8 cases, radar echoes were inadequately developed, suggesting insufficient charge accumulation. On the other hand, the remaining 3 cases had well-developed radar echoes, and there was no significant difference from the detection cases.

Plain Language Summary Gamma-ray glow is a minute-lasting burst of high-energy photons associated with thunderclouds. High-energy photons are considered to originate from high-energy electrons accelerated and multiplied in strong electric fields inside thunderclouds. When a gamma-ray glow is detected on the ground, electrons are considered to be accelerated downward by upward electric fields. In the 2020–2021 winter season, we detected a total of 6 gamma-ray glows during winter thunderstorms at Kanazawa University, Japan. An electric-field monitor recorded negative electric fields at the surface during all the glow detections, indicating negative charges overhead. It suggests that the thunderclouds that produced the gamma-ray glows were strongly charged negatively, and a localized positive charge layer existed in the lower part to produce an upward electric field for downward electron acceleration.

1. Introduction

Quasi-stable electric fields (E-fields) in thunderclouds have been recognized as particle accelerators in the atmospheres, as predicted by Wilson (1925). These accelerators have been detected as one of the high-energy atmospheric phenomena called gamma-ray glow, a minute-lasting burst of high-energy photons (also referred to as thunderstorm ground enhancement (TGE) when detected on the ground). When electrons are accelerated to relativistic energies such as MeV, they interact with atmospheric nuclei and produce high-energy photons by bremsstrahlung. Wilson (1925) introduced runaway electron acceleration initiated by high-energy seed electrons. Such seed electrons were thought to be provided by β-decay nuclei in the atmosphere, but nowadays electrons of secondary cosmic rays are more common candidates. After the first formulation of the runaway acceleration regime, A. Gurevich et al. (1992) considered avalanche processes of electrons in the atmosphere, called relativistic runaway electron avalanche (RREA). In the RREA regime, the number of accelerated electrons is a function of the number of seed electrons, the strength of the E-field, atmospheric pressure, and acceleration length. In particular, it increases exponentially as the acceleration length increases. At the surface atmospheric

pressure, the runaway acceleration works at >216 kV m^{-1} (A. V. Gurevich & Zybin, 2001), and the RREA works at >284 kV m^{-1} (Dwyer, 2003). Afterward, Dwyer (2003) proposed an additional multiplication mechanism to RREA called relativistic feedback. Besides, acceleration of cosmic-ray electrons without multiplication has been also proposed as the modification of the cosmic-ray spectra (Chilingarian et al., 2012, 2014; Cramer et al., 2017). Three mechanisms have been examined in Monte-Carlo simulations to reproduce a large part of gamma-ray glow observations (Bowers et al., 2019; G. Diniz et al., 2022; G. S. Diniz et al., 2023; Kelley et al., 2015; Østgaard et al., 2019; Sarria et al., 2023).

Although the number of detections is still limited, gamma-ray glows have been observed by aircraft (Kelley et al., 2015; Kochkin et al., 2017, 2021; Østgaard et al., 2019), balloon (Eack & Beasley, 2015; Eack et al., 1996), mountain-top (Bowers et al., 2019; Chilingarian et al., 2010, 2019, 2022; Chum et al., 2020; Torii et al., 2009; Tsuchiya et al., 2009, 2012; E. Williams et al., 2022), and sea-level experiments (Hisadomi et al., 2021; Kuroda et al., 2016; Torii et al., 2002; Tsuchiya et al., 2007, 2011, 2013; Wada, Enoto, et al., 2021; Wada, Matsumoto, et al., 2021; Wada et al., 2018, 2019), after the first discovery by an F-106 aircraft (McCarthy & Parks, 1985; Parks et al., 1981). Some ground-based experiments have been routinely operated, and allow systematic investigations of gamma-ray glows/TGEs (Chilingarian et al., 2019, 2022; Wada, Matsumoto, et al., 2021). Aragats Space Environment Center in Armenia, located at 3,200 m above sea level on the slope of Mt. Aragats, is the location where TGEs have been detected the most frequently (Chilingarian et al., 2019, 2022). While mountain-top experiments have been performed for targeting summer thunderstorms, sea-level experiments have been performed for aiming at winter thunderstorms in Japan (Kuroda et al., 2016; Torii et al., 2002; Tsuchiya et al., 2007; Wada, Matsumoto, et al., 2021; Yuasa et al., 2020). The Hokuriku region in Japan, facing the Sea of Japan, is famous for the occurrence of winter thunderstorms (Ishii et al., 2014). Winter thunderstorms have several characteristics quite different from summer thunderstorms. The most important feature of gamma-ray glows is the low-charge-center structure of thunderclouds. As the −10°C altitude, where electrification is the most efficient gets lower than 3 km (Kitagawa, 1992; Kitagawa & Michimoto, 1994; Takahashi et al., 2019; Yoshida et al., 2018), high-energy photons are less attenuated in the atmosphere than higher-charge-center summer thunderstorms, and hence gamma-ray glows are detected at sea level.

Besides radiation measurements, monitoring E-fields plays an important role in investigations of gamma-ray glows. Hereafter, we employ the sign convention of atmospheric electricity; negative values mean upward surface E-fields (electrons are accelerated downward). There are coordinated observations with radiation and E-field measurements. In-situ measurements of E-fields can be done by aircraft and balloon flights. Eack et al. (1996) performed a simultaneous measurement of X-ray counts and E-fields by balloon flights (Eack and Beasley (2015) revisited the observation result of Eack et al. (1996)). The increases in X-ray counts occurred when ambient E-field (both negative and positive) reached two-thirds of the runaway threshold (216 kV m^{-1} at sea level). On the other hand, it is generally difficult to make observations in a precipitation core as balloons tend to avoid such a downdraft region. Østgaard et al. (2019) observed a gamma-ray glow when an ER-2 aircraft was flying at an altitude of 20 km, above a thundercloud. Photon counts were measured together with two-dimensional E-field monitoring, and a charge structure of the upper part of the thundercloud was estimated.

Due to a large number of detections, E-field variations during gamma-ray glows/TGEs have been systematically investigated by ground-based experiments. The Armenian group has documented the largest number of TGEs with E-field measurements by field mills (Chilingarian et al., 2019, 2022). TGEs have been detected during both positive and negative surface E-fields. Recently, E. Williams et al. (2022) has given a relation between surface E-field polarity and radar-echo structures for TGEs at Mt. Aragats. With the assumption of the conventional tripolar structure of charge layers inside thunderclouds, they concluded that TGEs with negative surface E-fields originate from thunderstorms with deep convections, and TGEs with positive E-fields from thunderstorms with shallow convections. Also, TGEs with both negative and positive E-fields have been observed at Lomnicky Stit in Slovakia (Chum et al., 2020; Kudela et al., 2017).

In 2006, the Gamma-Ray Observation of Winter Thunderclouds (GROWTH) experiment started sea-level observations at Kashiwazaki-Kariwa Nuclear Power Plant, Japan, targeting high-energy atmospheric phenomena in winter thunderstorms. Several gamma-ray glows were reported with E-field measurements (Tsuchiya et al., 2007, 2011). In 2016, the GROWTH collaboration started a mapping observation campaign in Kanazawa, Japan (Yuasa et al., 2020). The positions of Kanazawa and Kashiwazaki are indicated in Figure 1. Thanks to the increased number of radiation monitors, a total of 70 gamma-ray glows were detected during four winter seasons

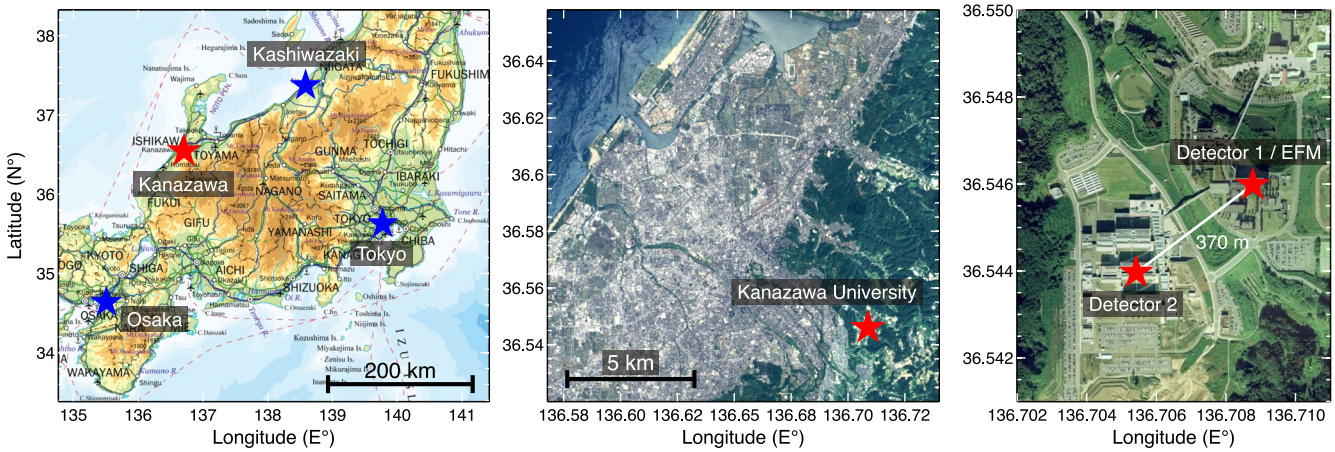

Figure 1. Maps of the detection sites at Kanazawa University. Left: the location of Kanazawa in the main island of Japan. Center: the location of Kanazawa University in the city of Kanazawa. Right: the location of Detector 1 and Detector 2, installed on different buildings at Kanazawa University. The field mill was installed beside Detector 1. The background images are provided by the Geospatial Information Authority of Japan.

(Wada, Matsumoto, et al., 2021). On the other hand, no field mills were installed beside the radiation monitors, and hence there are no systematic studies on the relation between gamma-ray glows and E-fields in winter thunderstorms, except for one case detected at the tip of Noto Peninsula (Wada et al., 2018). Then, we installed field mills at selected observation sites of our monitoring network after 2020. In this paper, we present the first result of systematic studies on gamma-ray glows and E-field variations during winter thunderstorms in Kanazawa. Also, we investigate non-detection cases with large E-field variations to compare with glow-detection cases. Hereafter, time is described in the Coordinated Universal Time (UTC) in principle, and also in the Japan Standard Time (JST: UTC + 9) if noted.

2. Instrumentation

The GROWTH collaboration launched the mapping observation campaign in 2016, and up to 10 portable detectors were distributed to universities, high schools, public facilities, and private companies around Kanazawa (Wada, Matsumoto, et al., 2021; Yuasa et al., 2020). Kanazawa is one of the urban areas in the Hokuriku region, facing the Sea of Japan, and is hit by winter lightning the most frequently among main cities in Japan (Japan Meteorological Agency, 2023a).

In the present paper, we focus on observation data obtained at Kanazawa University Kakuma Campus, one of our observation sites. From the 2016–2017 to 2019–2020 winter seasons, the largest number of gamma-ray glows were detected there (Wada, Matsumoto, et al., 2021). The location of Kanazawa University is shown in Figure 1. It is located ∼10 km east of the coast. Since November 2020, two radiation monitors have been installed at the campus. They are installed on the roof of two separate buildings and 370 m away from each other. The installation geometry is shown in the right panel of Figure 1. Hereafter, the detecter at the northeast is called Detector 1, and the other Detector 2. Each radiation monitor has a $Be_4Ge_3O_{12}$ (BGO) scintillation crystal of 25.0 cm3 × 8.0 cm3 × 2.5 cm^3 which is coupled with two R1924 photomultipliers of Hamamatsu. The output signals from the photomultipliers are digital-sampled, processed, and stored by our signal processing unit composed of a field-programmable gate array and a Raspberry Pi (Yuasa et al., 2020). While distinguishing energetic electrons from high-energy photons is becoming important (Chilingarian et al., 2022; E. Williams et al., 2022), our detectors did not have the ability to discriminate electrons from photons at this time.

A field mill was also installed beside Detector 1 in December 2020. We utilized MEF2R-1 of Otowa Electric Co., Ltd. It monitors E-fields with a range of up to ±210 kV m^{-1} (before plain-surface calibration) every 50 ms. The absolute timing is provided by global positioning system signals. Plain-surface calibration is performed with observation data during fair weather, assuming that E-field is typically ∼0.1 kV m^{-1} in fair weather. The Kanazawa local observatory (N36.588°, E136.633°) of Japan Meteorological Agency (JMA) reported sunny from 01:00 to 06:00 UTC (10:00–15:00 JST) on 20 January 2021. Also, we checked optical images of the Himawari

meteorological satellite, and no clouds covered Kanazawa. Then, an averaged value of E-fields between 02:00–05:00 UTC (11:00–14:00 JST) is normalized to be 0.1 kV m^{-1}. This is a rough calibration (the uncertainty could be ∼50%), but sufficient in the present paper because the absolute values of E-fields are not compared with other measurements. Both the field mill and the radiation monitors were in operation from 9 December 2020, to 19 March 2021.

A disdrometer (Persivel-2 of OTT HydroMet) was installed next to Detector 2. It measures the diameter and drop velocity of precipitation particles, then provides the type of the particles. The operation of the disdrometer was unstable, and observation was performed in limited periods. We also utilize an X-band dual-polarization radar of the eXtended RAdar Information Network (XRAIN), operated by the Ministry of Land, Infrastructure, Transport and Tourism. The X-band radar (Noumi station) is installed 17.1 km southwest of Kanazawa University. Its beam width and the center frequency are 1.2° and 9.785 GHz, respectively. A full-volume scan with 12 elevation angles completes in 5 min. The radar data is also utilized to estimate the wind direction and velocity by the pattern-matching technique. Considering the elevation angle of the X-band radar, the estimated wind information is at ∼1-km altitude.

We refer to the meteorological model, surface observation, and lightning data. The altitude of −10°C, where convection and charging are the most active, is derived from the mesoscale model (MSM) produced by JMA every 3 hr (Japan Meteorological Agency, 2023b). We utilize initial analysis data of MSM, not prediction data. The spatial resolution of MSM is 0.1° (latitude) and 0.125° (longitude), and data at the closest grid to the observation site (centered at N36.6°, E136.625°) is employed. The surface temperature data is measured at the Kanazawa local observatory of JMA. The LIghtning DEtection Network (LIDEN) data provided by JMA is also utilized to estimate the flash rate. LIDEN consists of 30 stations in Japan, recording low-frequency pulses of lightning discharges, and two-dimensionally locates the pulses by the time-of-arrival and magnetic-direction-finder techniques. The method to derive flash rate is the same as Wada, Tsurumi, et al. (2023); total lightning flashes (both cloud-to-ground and in-cloud flashes) are counted from 5 min before to 5 min after the glow detection in a 20 km × 20 km region centered at the detection site, and then the number of flashes is divided by the 10 min.

3. Glow-Detection Cases

The event survey was performed as follows (as performed in Wada, Matsumoto, et al. (2021)). Count-rate histories of >3 MeV were produced with a bin width of 60 s. The energy range of >3 MeV is dominated by cosmic-ray air showers, and hence is not affected by the background variations of radon-chain nuclei correlated with rainfall. The average and standard deviation of the count rates were calculated every 24 hr, and then count rates corresponding to >5 standard deviations (5σ) were surveyed. The 5σ threshold corresponds to ∼26% increase in count rates from the background level with our BGO scintillation crystals, when employing a 60-s binning. When a significant increase in the count-rate histories ($>5\sigma$) was found, we manually checked the count-rate history to verify the detection of gamma-ray glows. This detection process was performed for both Detectors 1 and 2 independently.

As a result, a total of 6 gamma-ray glows were detected during the operation period in the 2020–2021 winter season, Figure 2 presents the count-rate histories, relative increases in count rates from the background level, and the corresponding variations of the surface E-field. To calculate the relative increases in count rates, the background level is derived from the count rates 10 to 5 min before the glow detection (a total of 5 min). The detection time is summarized in Table 1. All the gamma-ray glows were significantly ($>5\sigma$) detected by both Detectors 1 and 2. Hereafter, the detected glows are numbered GG1–GG6. Based on the classification method of count-rate histories by Wada, Matsumoto, et al. (2021), GG5 is the double-peak type, and the others are categorized to be the single-peak temporally symmetric type. GG5 is the most prominent glow among the 6 cases, whose count rates reached ∼15 times of the background level (>3 MeV) recorded by Detector 2. The photon number of >3 MeV and duration are also summarized in Table 1. The duration is defined to be T80, the duration including 80% of the detected photons. A similar concept, T90, is often employed in gamma-ray astronomy (Zhang & Choi, 2008). The method to derive the photon number and duration is the same as Wada, Matsumoto, et al. (2021). The uncertainty of the photon-number estimation is caused by background estimation. Note that no downward TGFs were detected in conjunction with the gamma-ray glows.

As well as Figures 2 and 3 shows the E-field variations around the moment of glow detections. A common feature is negative E-field excursions during glow detections. The peak surface E-field at the glow detections, summarized in Table 2, is stronger than around −12 kV m^{-1}, except for GG6.

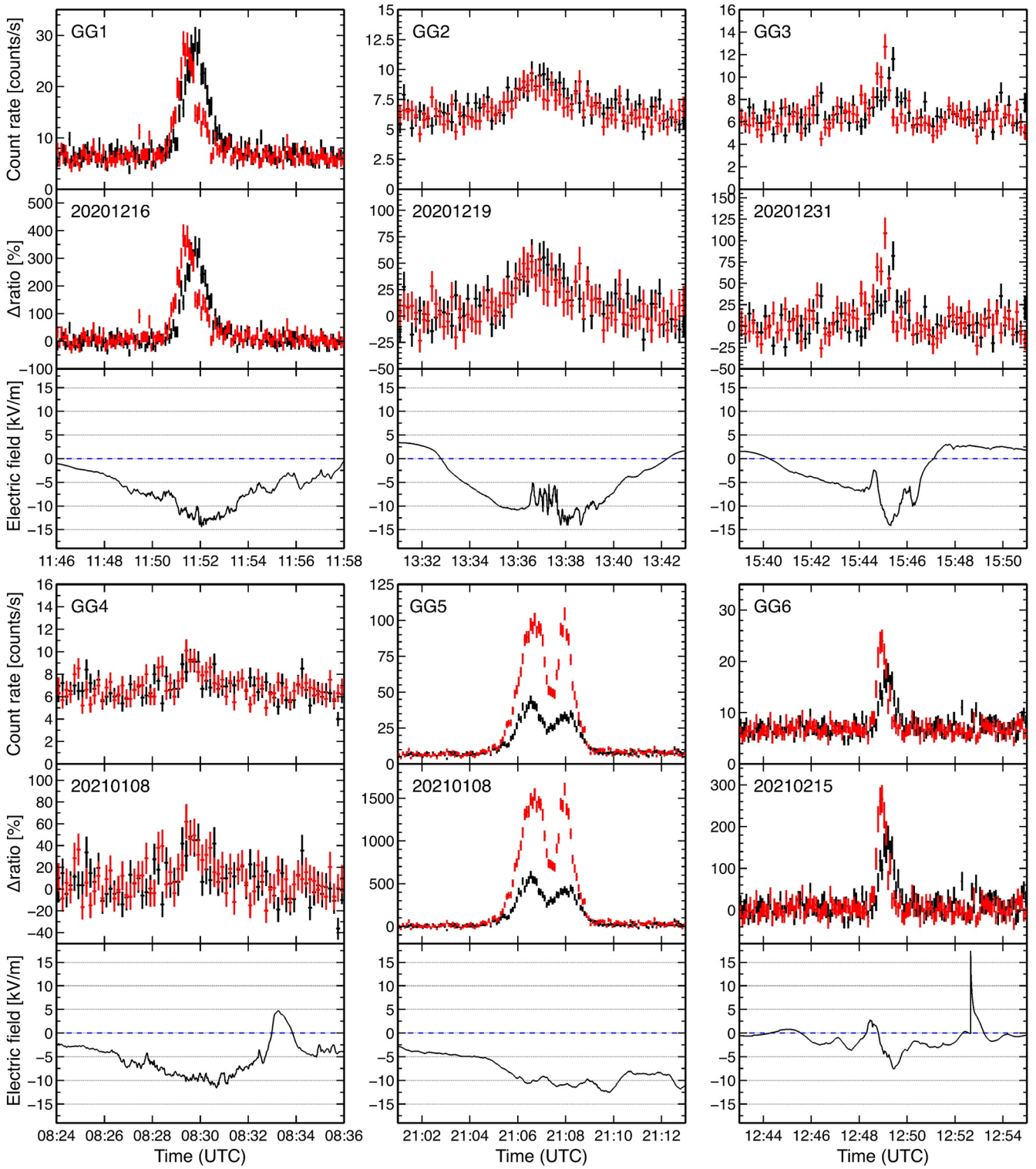

Figure 2. Count-rate histories, relative variations in count rates from the background level, and surface E-field variations of gamma-ray glows. The black and red data points of the count-rate histories indicate Detectors 1 and 2, respectively. In the relative variations in count rates, the background level is defined to be 0%. The surface E-fields were measured at the same position as Detector 1. The blue dashed lines of the surface E-field variations indicate 0 kV m^{-1}.

Table 1
List of Glow-Detection Cases

ID	Time (UTC)	Type	Significance (Detector 1/2)	Photon number (Detector 1/2)	Duration (s) (Detector 1/2)
GG1	2020-12-16 11:52	Symmetric	52.8σ/45.3σ	1,521 ± 45/1,357 ± 44	82/81
GG2	2020-12-19 13:37	Symmetric	8.3σ/7.7σ	531 ± 56/423 ± 55	231/182
GG3	2020-12-31 15:45	Symmetric	8.0 σ/9.5σ	215 ± 25/305 ± 35	68/87
GG4	2021-01-08 08:30	Symmetric	5.6σ/7.3σ	236 ± 44/275 ± 44	147/135
GG5	2021-01-08 21:07	Double peak	88.4σ/239.1σ	4,777 ± 53/11,917 ± 53	150/136
GG6	2021-02-15 12:49	Symmetric	18.6σ/25.6σ	392 ± 37/509 ± 37	41/31

GG1 shows a moderate convex E-field variation, and its peak time almost coincides with that of the gamma-ray count at Detector 1. In GG2, the peak time of the E-field variation is about 1 min after that of the gamma-ray count, and the E-field shows small fluctuations at the peak of the gamma-ray count. In GG3, the peak time of the gamma-ray count coincides with that of the E-field variation, showing a convex feature on a timescale of about 1 min. GG4 shows a moderate convex E-field variation with a peak about 1 min after the count-rate peak of the gamma-ray glow. GG5 is the only double-peak type among the six cases. Two local convex variations, corresponding to the two gamma-ray peaks, are seen in the E-field variation. Afterward, a third convex variation is seen from 21:09 to 21:10, and the peak value is larger than the preceding two convex variations. On the other

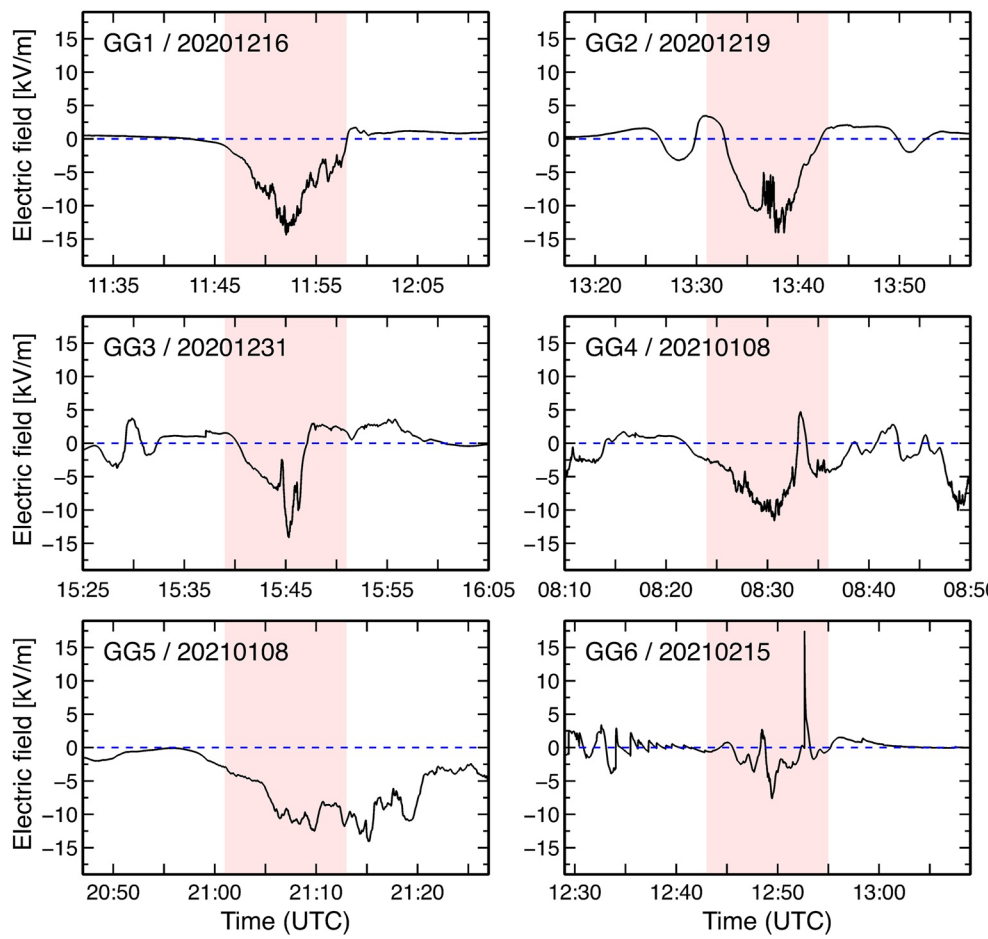

Figure 3. E-field variations around the moment of glow detections, with a longer time scale than Figure 2. The blue dashed lines indicate 0 kV m^{-1}. The pale-pink shaded areas show the display range of Figure 2.

Table 2
Meteorological Parameters of Glow-Detection and Non-Detection Cases

ID	Time (UTC)	Peak surface E-field (kV/m)	Temp. at surface (°C)	Altitude at −10°C (km)	Flash rate (flash/min)	Wind		Precipitation[a] particle
						Direction (°)	Speed (m/s)	
Glow-detection cases								
GG1	2020-12-16 11:52	−14.4	2.4	1.5	0.0	300	12.1	+GS/+SN
GG2	2020-12-19 13:37	−14.1	1.6	1.6	0.0	300	12.1	+GS/−GS/−SN
GG3	2020-12-31 15:45	−14.1	2.8	1.6	0.0	270	21.2	No data
GG4	2021-01-08 08:30	−11.6	0.7	1.3	0.0	270	15.7	No data
GG5	2021-01-08 21:07	−12.2	−0.4	1.3	0.0	270	14.6	No data
GG6	2021-02-15 12:49	−7.6	8.4	2.6	0.0	260	28.5	No data
Non-detection Cases								
ND1	2020-12-15 03:58	−12.1	4.2	1.6	0.0	280	13.7	+GS/GS
ND2	2020-12-25 07:30	−13.2	5.8	2.0	0.0	270	17.2	RASN/RA/+GS
ND3	2021-01-01 00:22	−13.2	2.6	1.6	0.0	270	18.0	No data
ND4	2021-01-01 06:28	−14.5	4.0	1.6	0.0	270	17.0	No data
ND5	2021-01-07 12:05	−13.0	−0.9	1.1	0.0	300	10.7	No data
ND6	2021-02-08 08:54	−12.8	0.7	1.4	0.0	350	8.6	No data
ND7	2021-02-08 15:46	−12.5	−0.6	1.2	0.0	302	9.8	No data
ND8	2021-02-18 03:21	−15.4	0.3	1.3	0.0	270	12.0	+SN/SN

[a]Detected within a total of 3 min, 1 min before and after the detection time of gamma-ray glows. Indicated by METAR Table 4678. RA, SN, RASN, and GS represent rain, snow, rain or drizzle with snow, and soft hail, respectively. Symbols with prefixes +, −, and without a prefix mean heavy, light, and moderate precipitation, respectively.

hand, the gamma-ray glow had already passed by this time, and no gamma-ray glow corresponding to the third E-field peak was found. Also seen in Figure 3, there is a negative E-field variation with three more peaks after the three peaks. The values of the succeeding E-field peaks are larger than those at the time of the glow detection, but no gamma-ray glow was detected at this time. In GG6, the E-field shows a positive peak just before the gamma-ray glow, but then it suddenly changes to negative and reaches a negative peak almost coincident with the peak time of the gamma-ray count. The negative peak value is −7.6 kV m^{-1} and is exceptionally weak in the six glow cases. About 4 min after the gamma-ray glow, a pulse-like E-field change originating from a lightning discharge was recorded.

Figure 4 shows the E-field variations for 6 hr centered on the detection time. In all the glow-detection cases, significant E-field changes were measured at moments other than the glow-detection time. On the other hand, in the time period of 3 hr before and after, the negative E-field variations around the detection time of the gamma-ray glows are the strongest, excluding the pulses originating from lightning discharges. Furthermore, the peak negative fields clearly dominate over peak positive fields in these periods. In GG6, rather large-amplitude E-field variations can be seen at around 12:20, but these are bursts of pulse-like E-field changes probably originating from multiple lightning discharges. Note that lightning flashes, especially in-cloud flashes in winter thunderstorms, can be missed by lightning location systems including LIDEN.

Figure 5 shows the plan-position-indicator (PPI) scans of radar echoes obtained by the Noumi X-band radar when the gamma-ray glows were detected, and Figure 6 shows the range-height-indicator (RHI) views composed of multiple PPI scans with 12 elevation angles. In all the cases, the PPI scans show that a strong echo region exceeding 35 dBZ is approaching the observation site. In addition, the RHI charts show that such a strong echo region has developed up to an altitude of 2–3 km, and that an active convective thundercloud passed just above the detection site. These characteristics are consistent with the detection cases at Kanazawa University (the same site as the present study), reported by Wada, Enoto, et al. (2021).

Table 2 summarizes meteorological parameters such as surface temperature, −10°C altitude, flash rate, wind speed, and wind direction at the moment of the glow detections. The −10°C altitude of GG1 to GG5 is 1.3–1.6 km,

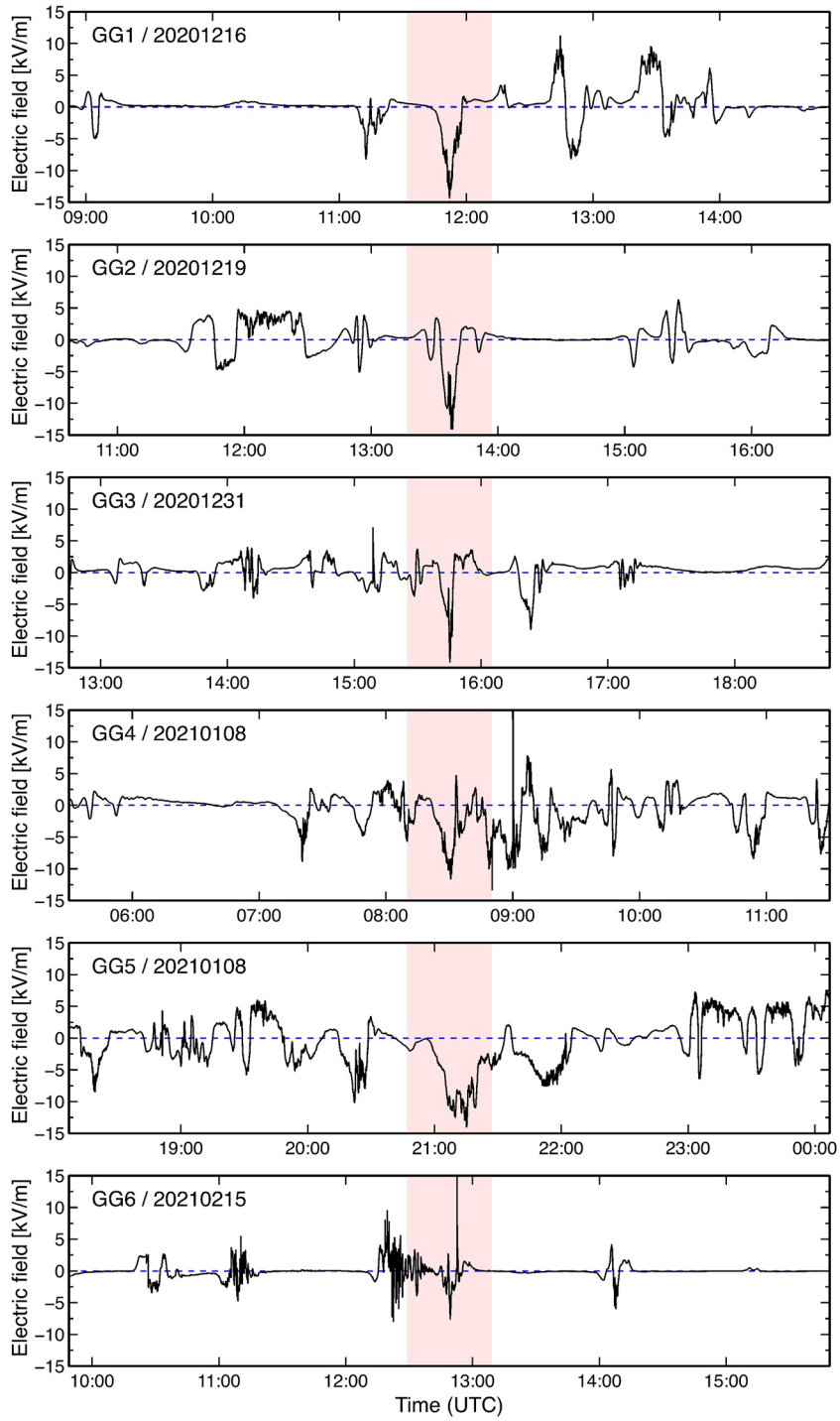

Figure 4. Overviews of E-field variations around the moment of glow detections. The pale-pink shaded areas correspond to the display range of Figure 3.

while that of GG6 is 2.6 km, exceptionally high. Likewise, the surface temperature of GG6 is 8.4°C, which is higher than in the other cases. The wind direction is west-northwest for GG1 and GG2, and west for GG3–GG6.

The flash rate was 0 flashes s^{-1} for all the glow-detection cases; LIDEN detected no lightning discharges in the 20-km square area centered at the detection site for 5 min before and after the glow-detection time. Four minutes after GG6, a pulse-like E-field variation originating from a lightning discharge was detected. In fact, LIDEN

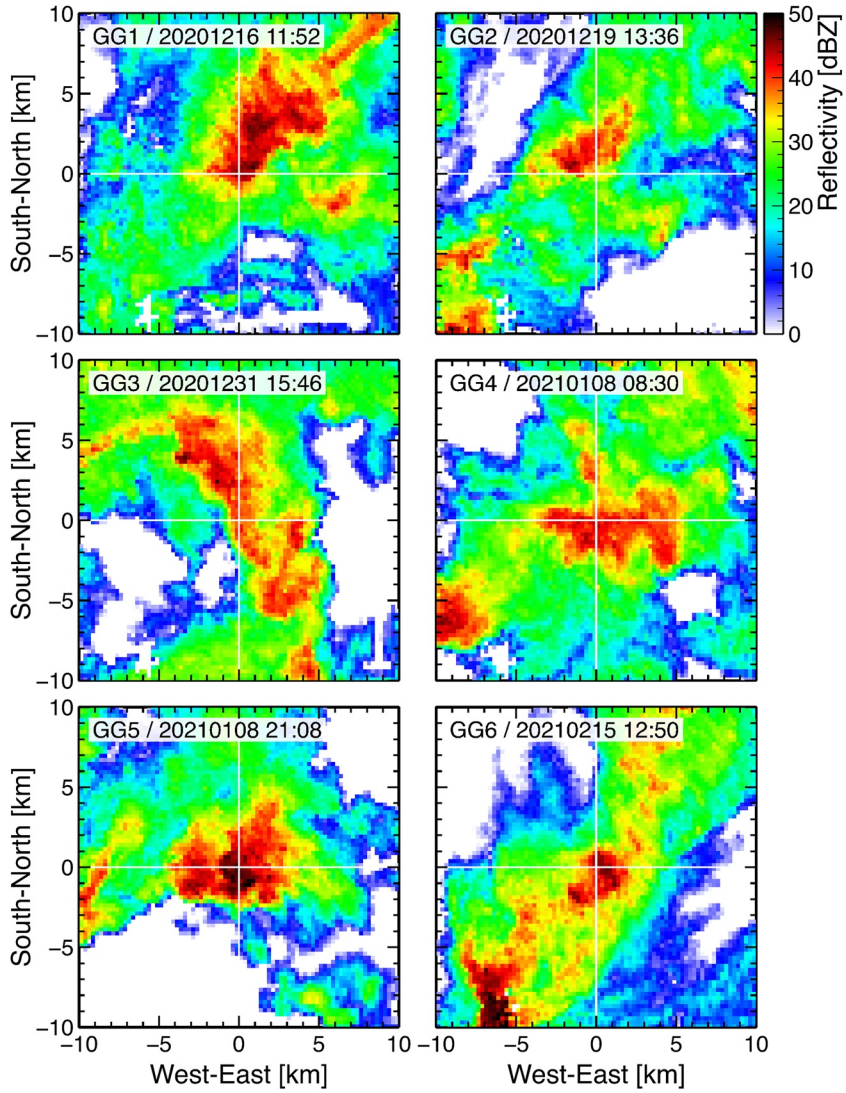

Figure 5. Plan-position-indicator views of radar echoes obtained by the Noumi X-band radar at the moment of the glow detections. The crossing point of the two white lines shows the observation site (Kanazawa University). The elevation angle is 3.6°, corresponding to 1.1-km altitude at the detection site.

detected a cloud-to-ground lightning flash at 12:52:42. However, this flash is not counted for the flash rate as it was located farther than 10 km from the observation site, outside of the 20-km square area. Precipitation particles observed by the disdrometer are also summarized in Table 2. Graupel and snow particles were detected in GG1 and GG2 for 3 min around the detection time. The disdrometer was not in operation at the moment of GG3–GG6 unfortunately.

4. Non-Detection Cases

In addition to the six glow-detection cases in the 2020–2021 winter season, we also investigated non-detected cases of gamma-ray glows. Non-detection cases were identified when the surface E-field was stronger than -12 kV m^{-1}. Pulse-like variations due to lightning discharges were excluded. Eight non-detection cases were found during the operation period of the detector, hereafter called ND1–ND8, respectively. The time and meteorological parameters of the non-detection cases are also summarized in Table 2. Figure 7 shows the E-field variations of the non-detection case. In all the cases, a negative convex E-field change lasting for about 5 min is seen. In ND5, a strong positive E-field variation is seen before the negative E-field variation.

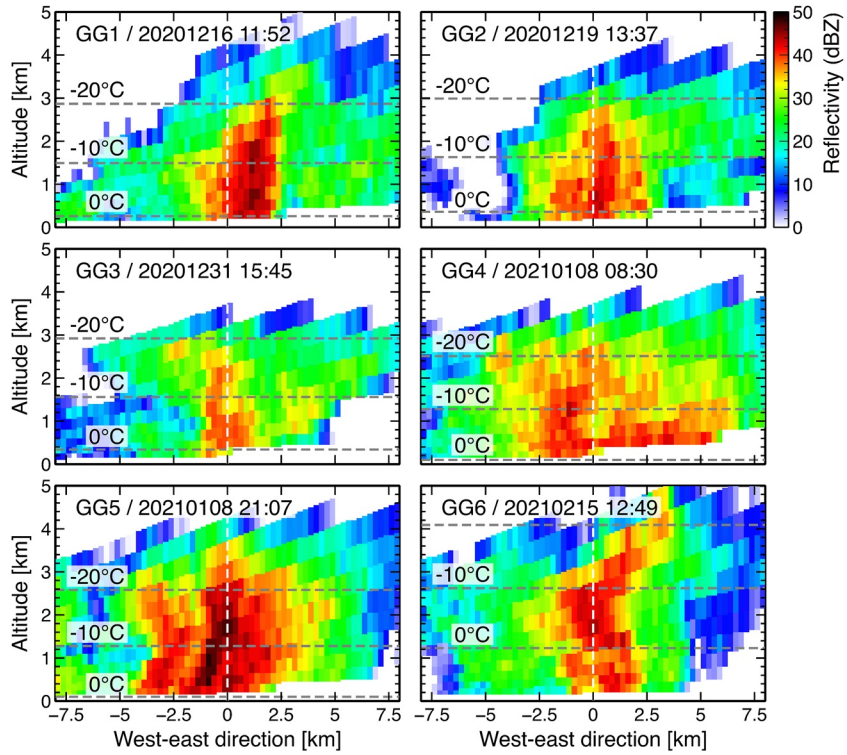

Figure 6. Range-height-indicator cross-sections of radar echoes composed of 12 plan-position-indicator scans by the Noumi X-band radar at the moment of the glow detections. The movement of radar echoes by wind flow, due to the difference in scan timing, is corrected. The white dashed lines show the observation site. The gray dashed lines indicate the altitude of 0°C, −10°C, and −20°C, derived with the mesoscale model.

Figures 8 and 9 show PPI and RHI views of the non-detection cases obtained by the Noumi X-band radar. In ND1–ND4, a strong echo over 35 dBZ was seen in the PPI scan. In the RHI chart, convective cores that had developed to an altitude of more than 2 km were observed in ND2–ND4, suggesting that cumulonimbus clouds had passed over the observation site. In ND1, the echo region above 35 dBZ developed up to 1.5-km altitude and had a shallow convective feature, but the development of the convection was significantly weaker than that of ND2–ND4. ND5 and ND6 had a spreading echo region of 20–30 dBZ, as seen in the PPI scans. Since there is no developed area over 35 dBZ in the RHI charts, convection was hardly developed. In ND7 and ND8, a small strong echo can be seen at the detection site in the PPI scans. However, the altitude of the strong echo is about 1 km and the development of convection is weak, as shown in the RHI charts.

5. Discussion

5.1. Charge Structures Responsible for Electron Acceleration

The E-field structure in which electrons are accelerated is one of the major issues in the gamma-ray glow science. For gamma-ray glows detected on the ground, electrons must be accelerated downward; there must be an upward E-field between a positively charged region and a negatively charged region above it in the lower part of a thundercloud.

Although the charge structures of winter thunderclouds in Japan are diverse, as shown by Zheng et al. (2019), they typically exhibit inverted bipolar, normal bipolar, or tripolar structures. A simplified schematics of the three charge structures is shown in Figure 10. The inverted bipolar is a structure in which positive charges are accumulated in the lower part of a thundercloud and negative charges in the upper part. Saunders and Peck (1998) reported that graupels tend to be positively charged even at low temperatures under the condition of high riming accretion rates. This is one of the candidates for the charging mechanism that creates the inversed bipolar structure. In this bipolar structure, an upward E-field is formed in the thundercloud, creating an environment in which electrons are accelerated downward. However, the surface E-field should be positive due to the lower positive

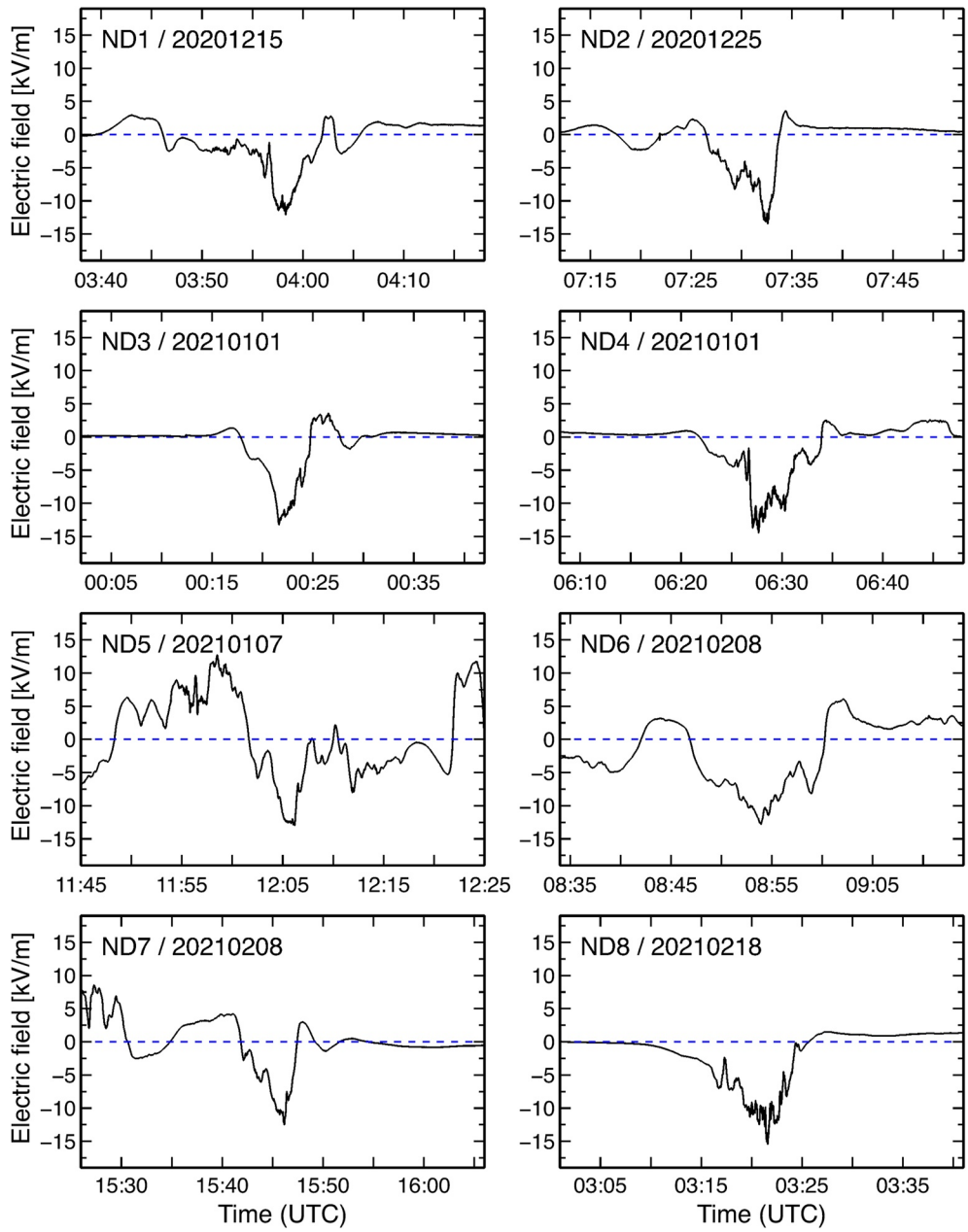

Figure 7. E-field variations around the moment of non-detection cases, in the same format as Figure 3.

charge layer and the negative image charges at the surface. This contradicts our observation that the surface E-field was negative during the detection of the gamma-ray glows. Therefore, the inverted bipolar structure cannot explain the gamma-ray glows in the present study.

In the normal bipolar structure, the lower layer of the thundercloud is charged negatively and the upper layer is charged positively. In this structure, a downward E-field is formed in the thundercloud, and electrons are not accelerated downward. On the other hand, an upward E-field is formed between the negative charge in the lower layer and the positive mirror charge on the surface, causing the electron to be directed downward. At this time, the surface E-field should be negative. The E-field is strongest just below the negative charge layer and gets weakened as approaches the surface. In addition, strong E-fields cannot be maintained near the surface due to corona discharge, and are hence limited up to around 10 kV m^{-1} (Rakov & Uman, 2003). This is consistent with the present observations in which the E-field is at most −15 kV m^{-1}.

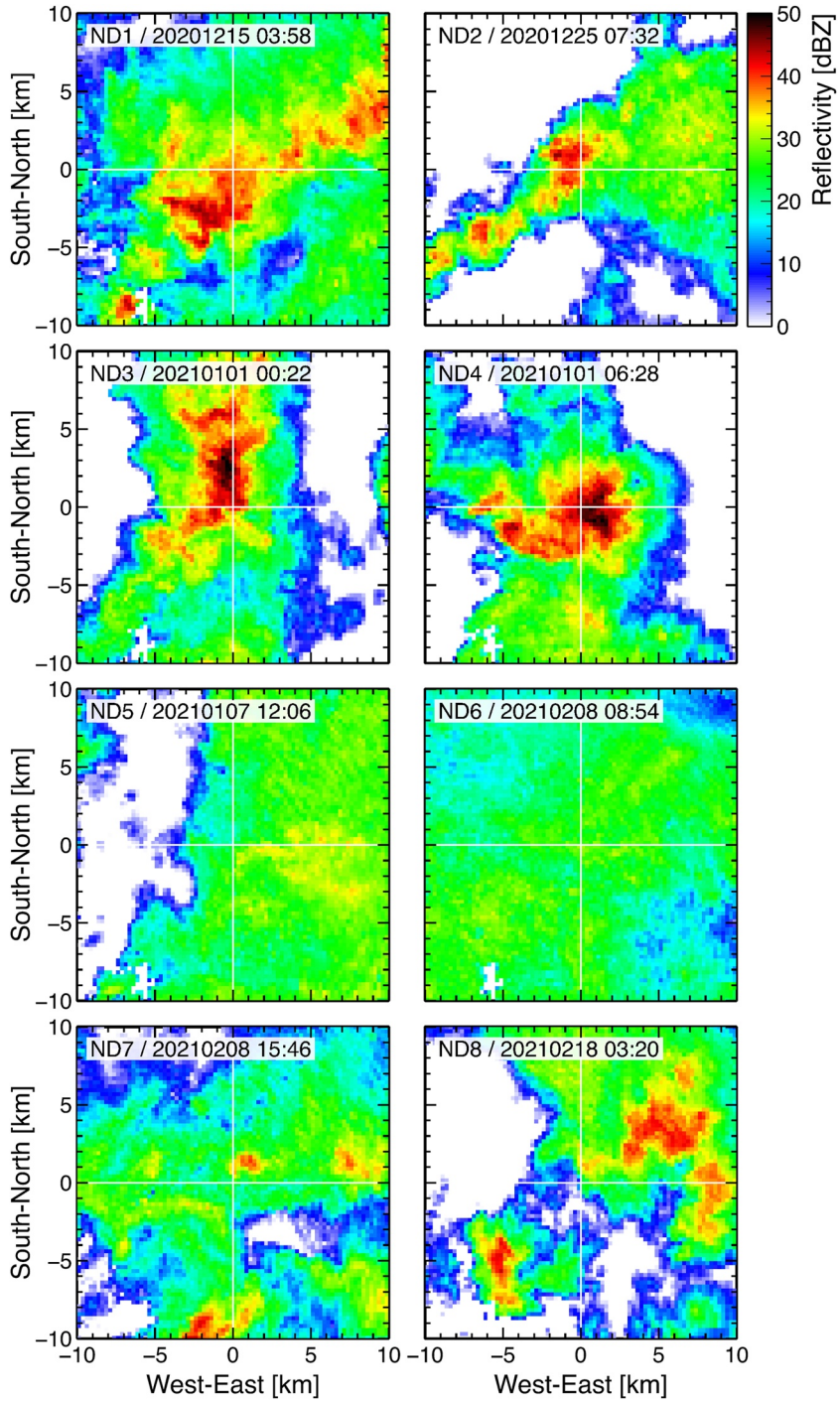

Figure 8. Plan-position-indicator views of radar echoes obtained by the Noumi X-band radar in the non-detection cases, in the same format as Figure 5.

An important point in the normal bipolar structure is that electron acceleration would occur in the E-field between the lower negative charge layer and the image positive charge at the surface. The E-field strength contributing to the electron acceleration should correlate with the surface E-field. In other words, electrons are more likely to be accelerated and multiplied as the surface E-field strength reaches its negative peak, and the gamma-ray flux on the ground should reach the maximum. In GG1 and GG3, the peak times of the E-field and gamma-ray flux coincide, which is consistent with this hypothesis. On the other hand, for the other four cases, the peak time of gamma-ray flux and the time when the E-field reached the negative peak do not match. In GG5, for example, the

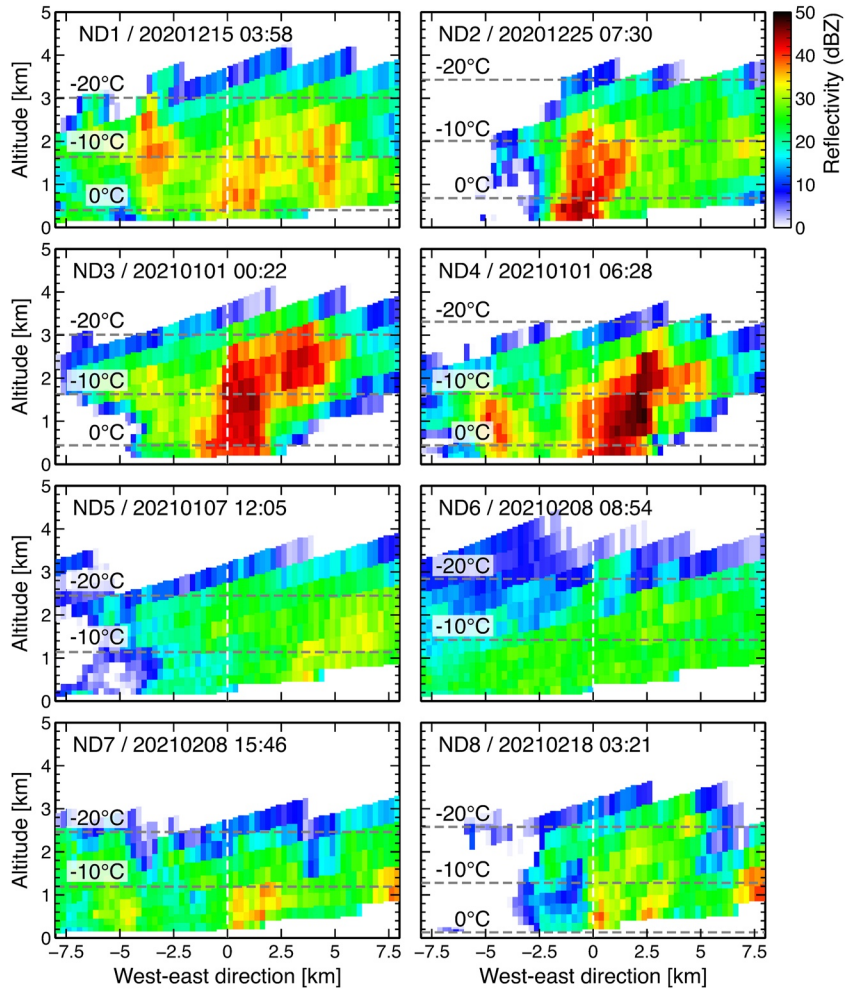

Figure 9. Range-height-indicator cross-sections of radar echoes by the Noumi X-band radar in the non-detection cases, in the same format as 6.

negative E-field became stronger around 21:10 than during the gamma-ray glow, but no gamma-ray glow was detected. Later, around 21:15, another stronger negative E-field was recorded, but similarly, no gamma-ray glow was detected.

It is also worth mentioning the tilted cloud structure in winter thunderstorms. Due to vertical wind shear, winter thunderclouds in Japan can be tilted, and the upper positive charge region can be exposed (Brook et al., 1982; Takeuti et al., 1978; E. Williams, 2018). As seen in Figure 6, GG6 probably presents a tilted cloud structure. This idea is supported by the positive E-field excursion preceding the negative E-field variation corresponding to the glow (see Figure 2). In this case, the time of the negative E-field peak could be affected by the exposed upper positive charges due to the tilted structure. Namely, the normal-bipolar hypothesis could work for GG6. Therefore, it is possible to explain GG1, GG3, and GG6 with the normal dipolar structure.

The tripolar structure is a typical E-field structure in summer thunderclouds (E. R. Williams, 1989), but it is also one of the typical charge models in winter (Brook et al., 1982; Takahashi et al., 1999, 2017, 2019). A middle negative layer and an upper positive layer are the main charge layers, and a local positive charge region (LPCR) is formed below the negative layer. An upward E-field is formed between the middle negative layer and the LPCR, and electrons can be accelerated downward. Electron acceleration by the upward E-field has been often discussed (e.g., Chilingarian & Mkrtchyan, 2012; E. Williams et al., 2022). As shown in Kitagawa and Michimoto (1994), the surface E-field below thunderclouds with the tripolar structure first becomes negative due to the negative charge layer, approaches positive as the LPCR reaches, and then returns to negative again when the LPCR passes.

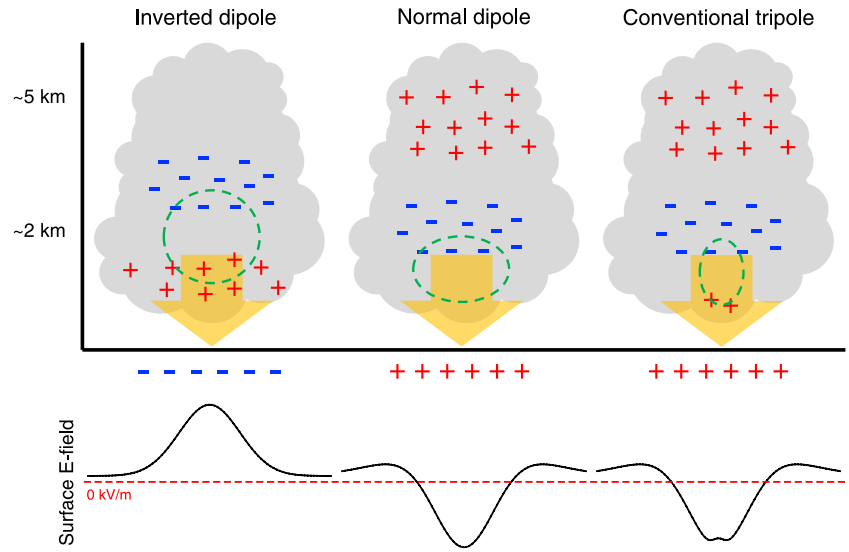

Figure 10. Simplified schematics of three charge structures in a thundercloud and corresponding changes of surface E-fields. Possible electron-accelerating regions are indicated by the green circles. The orange arrows show the direction of electron acceleration and the gamma-ray motion.

This fluctuation is referred to as a "W-type" variation. In particular, the E-field can temporarily become positive when the LPCR with a large amount of positive charge reaches directly above the detector. Also, the LPCR could be developing and manifest at the surface when a downdraft begins (Lhermitte & Williams, 1985). Active thunderclouds with a large amount of positive charge are often seen at the beginning and end of the winter season, such as November and March, and are more likely to be accompanied by frontal thunderclouds with high temperatures compared to thunderstorms in midwinter (Kitagawa & Michimoto, 1994). E. Williams (2018) also mentioned that the "snow dipole", where snow aggregates are dominant for electrification, could play an important role for midwinter thunderstorms.

In the present study, the surface E-field in GG2 gets closer to the positive side compared to before and after the peak time of the gamma-ray flux (Figure 2). Pulsed E-field fluctuations were recorded during the detection of the gamma-ray glow, likely due to weak lightning discharges or corona discharges, and it is unclear whether these E-field fluctuations to the positive side originate from the passage of the LPCR.

In the other cases, the E-field has a negative peak around the peak of the gamma-ray fluxes, and no clear W-shaped E-field fluctuation was detected. These cases are similar to negative TGEs (TGEs with negative E-field variation) detected at the Aragats Space Environment Center. E. Williams et al. (2022) analyzed that negative TGEs occur when vertical convection is active. It means that the upper positive and middle negative layers are dominant, and the amount of positive charge in the LPCR is relatively small. If the LPCR is localized and the middle negative layer is well developed, the effect of the LPCR to surface E-fields is relatively small, and hence the E-field fluctuation due to the LPCR becomes quite small or negligible. On the other hand, if a sufficient upward E-field is formed between the LPCR and the middle negative layer, electrons are accelerated downward and a gamma-ray glow can be detected on the ground. This model can consistently explain the E-field variation and the gamma-ray flux in all the detected cases.

In GG5, two peaks in the gamma-ray flux and corresponding variations in the surface E-field are seen. The E-field has a local minimum with respect to the first peak of the gamma-ray flux, and the peak times of the gamma-ray flux and the E-field coincide. On the other hand, the E-field corresponding to the second gamma-ray peak shows a small W-shaped fluctuation; the surface E-field shows a local maximum corresponding to the peak of the gamma-ray flux. It is possible that this E-field fluctuation originates from an LPCR.

In all the glow-detection cases, the negative E-field was the strongest in the interval including 3 hr before and after the detection time. This means that the middle negative charge layer is the most accumulated during the detection of the gamma-ray glows. Under such circumstances, the effect of the LPCR on the surface E-field is

relatively small. In the present cases, it is considered that the middle negative layer was well developed, and that an LPCR could have existed underneath when the gamma-ray glows were detected.

E. Williams et al. (2022) picked up 12 positive TGEs and 9 negative TGEs at Aragats. They concluded that positive TGEs occur when thundercloud convection is relatively weak and the underlying positive charge is abundant, while negative TGEs occur when thundercloud convection is relatively active. Thus, surface E-field fluctuations of both polarities have been recorded during TGEs at Aragats. However, no gamma-ray glows accompanied by positive E-fields were detected in the present study. The reason why gamma-ray glows with positive surface E-fields are not detected in winter thunderstorms is unknown at present. But this study shows only the results in one winter season, and future observations will enable statistical discussion.

Among the 6 cases, the peak value of the surface E-field in GG6 is exceptionally small. The −10°C altitude was 1.3–1.6 km in the other cases, but that in GG6 was 2.6 km, exceptionally high, and the temperature at surface was also high. Wada, Tsurumi, et al. (2023) reported that there are glow-detection cases where the −10°C altitude exceeds 2 km and the surface temperature exceeds 8°C. Therefore, GG6 is not a special case. If the −10°C altitude is high, the altitude at which charge separation occurs is also high. For gamma-ray glows to be detected on the ground, the accelerating region, the strong E-field region between the LPCR and the middle negative layer must be close to the ground. Since the X-band radar recorded strong echoes near the ground, charged precipitation particles were likely to reach the ground and the strong E-field region was approaching the ground. On the other hand, the strong echo region exceeding 35 dBZ reached an altitude of 4 km or more, and the thundercloud was taller than in other cases. For this reason, most of the negative charges in the middle layer were still at around the −10°C altitude, the surface E-field formed by the middle negative layer and the positive image charge could have been smaller than in other cases.

5.2. Comparison Between Glow-Detection and Non-Detection Cases

In addition to the glow-detection cases, non-detection cases where the surface E-field was strong but gamma-ray glows were not observed, were also identified. The non-detection cases are classified into stratiform precipitation, weak convective precipitation, and strong convective precipitation. ND5 and ND6 are categorized into stratiform precipitation. On the radar images, a spreading echo of ∼30 dBZ is found, and the echo-top height is 3–4 km. The wind directions are west-northwest and northwest in ND5 and ND6, and the surface temperatures are 0.7°C and −0.6°C, respectively. Although the disdrometer was not in operation, the E-field fluctuates are considered to originate from snowfall because no bright band was detected.

In ND1, ND7, and ND8, strong echo regions of 35 dBZ or more passed near the observation site, as seen by the PPI images. However, the echo regions were not well developed in the direction of altitude as seen in the RHI images, and hence convection seemed to be weaker than in the glow-detection cases. In ND8, the disdrometer detected snow, and the E-field fluctuation seems to originate from snowfall, similar to ND5 and 6. It is thought that charges were not well accumulated enough to trigger lightning discharges.

ND2, ND3, and ND4 are classified as strong convective precipitation. In PPI images, it can be seen that the strong echo region passed over the detection site. In the RHI images, strong echo regions developed up to 2–3 km, indicating strong convection. These radar observations are not significantly different from the glow-detection cases. The surface temperature of the three cases was 2.6°C–5.8°C, and the −10°C altitude was 1.6–2.0 km, which is consistent with the glow-detection cases. Therefore, there is no difference between the three non-detection cases and glow-detection cases, as shown by surface E-field measurements, radar observations, and meteorological parameters.

To further investigate the development of storms in the glow-detection and non-detection cases, we extract time series of RHI images, 10 and 5 min before, at the moment of, and 5 min after the detection/non-detection time. Figure 11 shows the time series for the glow-detection cases, and Figures 12 and 13 for the non-detection cases. The latitude of the west-east cross-sections is moved with the estimated wind, assuming that the wind is constant during 20 min. It means that the time-series plots focus on the temporal development and eastward movement of the clouds. In all the glow-detection cases, the echo regions were decaying 5 min after the detections. Namely, the gamma-ray glows were detected during a passage of collapsing storms, as also seen in E. Williams et al. (2022). It could suggest that positively charged graupels and/or snow aggregates were falling, and the upward E-field responsible for the electron acceleration was descending. The same feature was also seen in another glow detected at the same site on 18 December 2018 (Wada, Wu, et al., 2023).

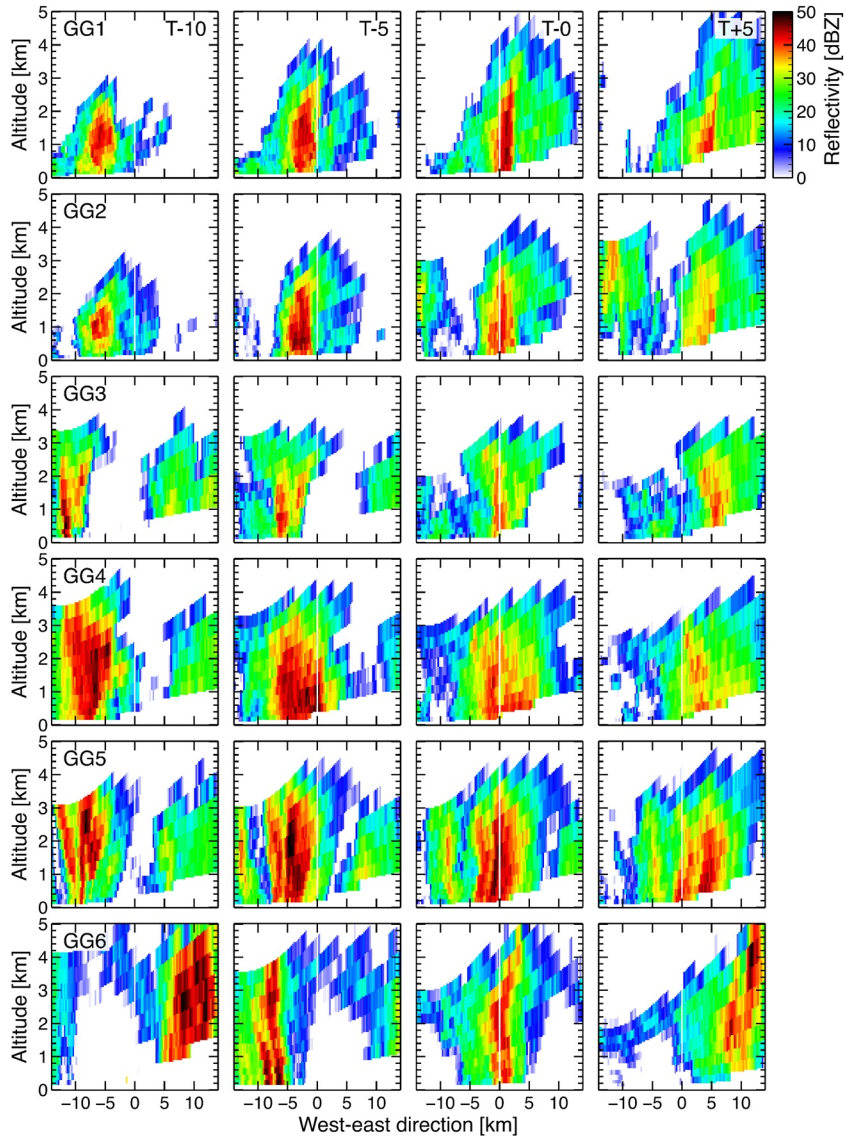

Figure 11. Time series of range-height-indicator cross-sections for the glow-detection cases, 10 and 5 min before, at the moment of, and 5 min after the glow detection.

In the non-detection cases, ND2, ND3, ND4 present descending echo regions, similar to the glow-detection cases. In particular, a collapsing feature is significant for ND2. Therefore, the difference between these non-detection cases and the glow-detection cases is still unclear, even though the temporal development of radar echoes are investigated. In ND1, a developing feature of the echo region associated with the negative E-field can be seen, but is weaker than the glow-detection cases and the three non-detection cases. The other non-detection cases, ND5–ND8, do not exhibit developing features of radar echoes.

Based on the LIDEN observation, the flash rates were calculated to be 0 flashes min^{-1} for both the glow-detection and non-detection cases. Wada, Tsurumi, et al. (2023) reported an average flash rate of 0.23 flashes min^{-1} for glow-detection cases in winter thunderstorms. Several cases in Wada, Tsurumi, et al. (2023) were associated with zero flash rates, and hence the present cases are not peculiar. On the other hand, flash rates cannot differentiate the glow-detection and non-detection cases in the present paper.

There are two hypotheses to explain why the conditions were the same between the glow-detection and non-detection cases. One is that there is no LPCR or the amount of positive charge is too small to cause electron acceleration. As mentioned above, the LPCR is important for the formation of the upward E-field, but it is

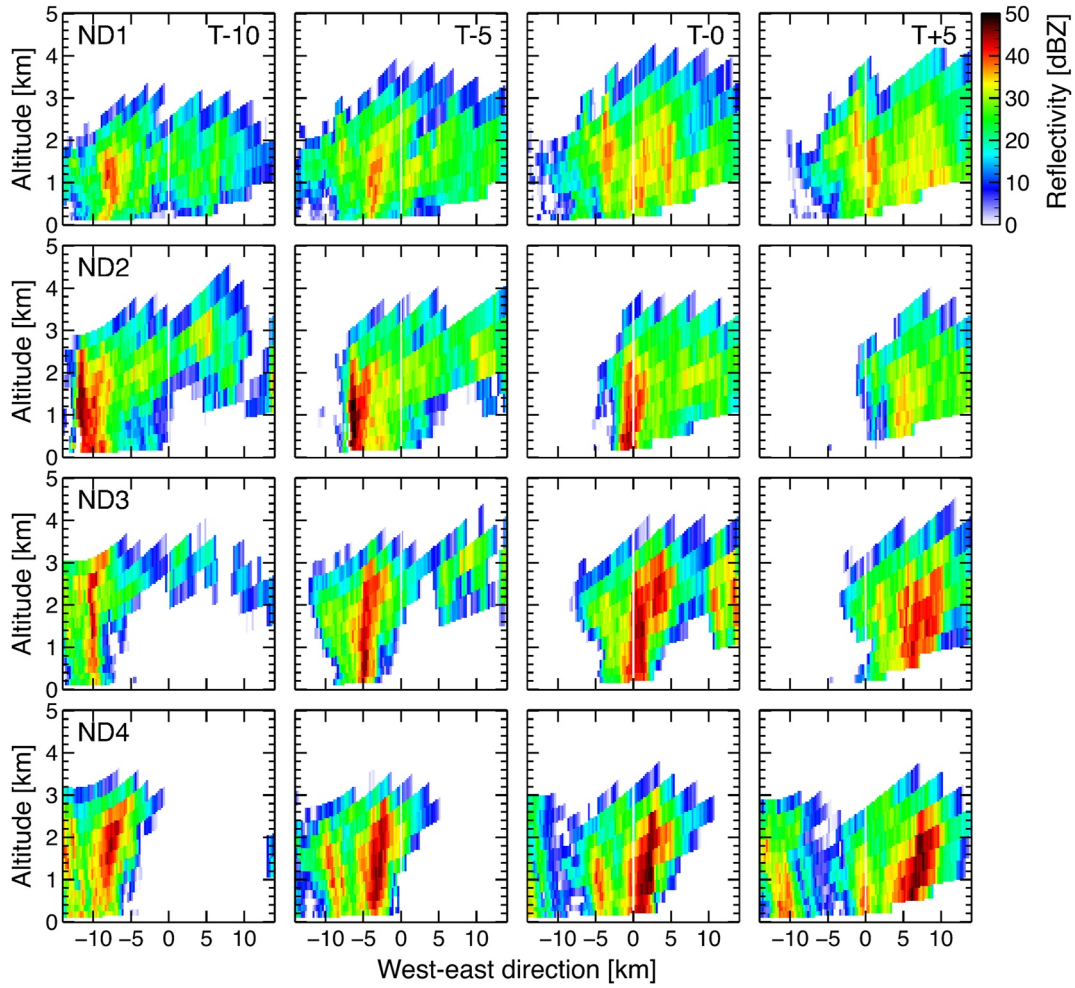

Figure 12. Time series of range-height-indicator cross-sections for the non-detection cases ND1–ND4, in the same format as Figure 11.

difficult to explicitly determine whether LPCRs exist by surface E-field observations. Since the glow cases are associated with collapsing storms with downdraft, it will be valuable to measure the polarity of precipitation particles to investigate the existence of LPCR.

Another possibility is that a gamma-ray glow existed, but the detector was far from the center of the gamma-ray glow and could not have caught the gamma-ray glow. In the present study, we installed two gamma-ray detectors at Kanazawa University. Since all the gamma-ray glows were detected simultaneously by the two detectors, the irradiation area of the gamma-ray glows on the ground should have a scale of at least 300 m or more. On the other hand, if the center of the gamma-ray glow passed several hundred meters north of Detector 1 or south of Detector 2, the detection network could have missed it.

6. Conclusion

We reported six gamma-ray glows with surface E-field measurements in the 2020–2021 winter season at Kanazawa University. All the gamma-ray glows were detected during the negative excursion of surface E-fields, and a passage of collapsing storms. The peak E-fields reach ~ -8 kV m^{-1} in GG6 and ~ -12 kV m^{-1} in the other cases, which is differentiated by surface temperature and -10°C altitude. Similarly to negative TGEs reported by E. Williams et al. (2022), the gamma-ray glows in the present studies can be explained by the tripolar charge structure in thunderclouds with a small LPCR. GG1, GG3, and GG6 can also be explained by the normal dipolar charge structure. Among the non-detection cases with E-field variations of < -12 kV m^{-1}, five were not associated

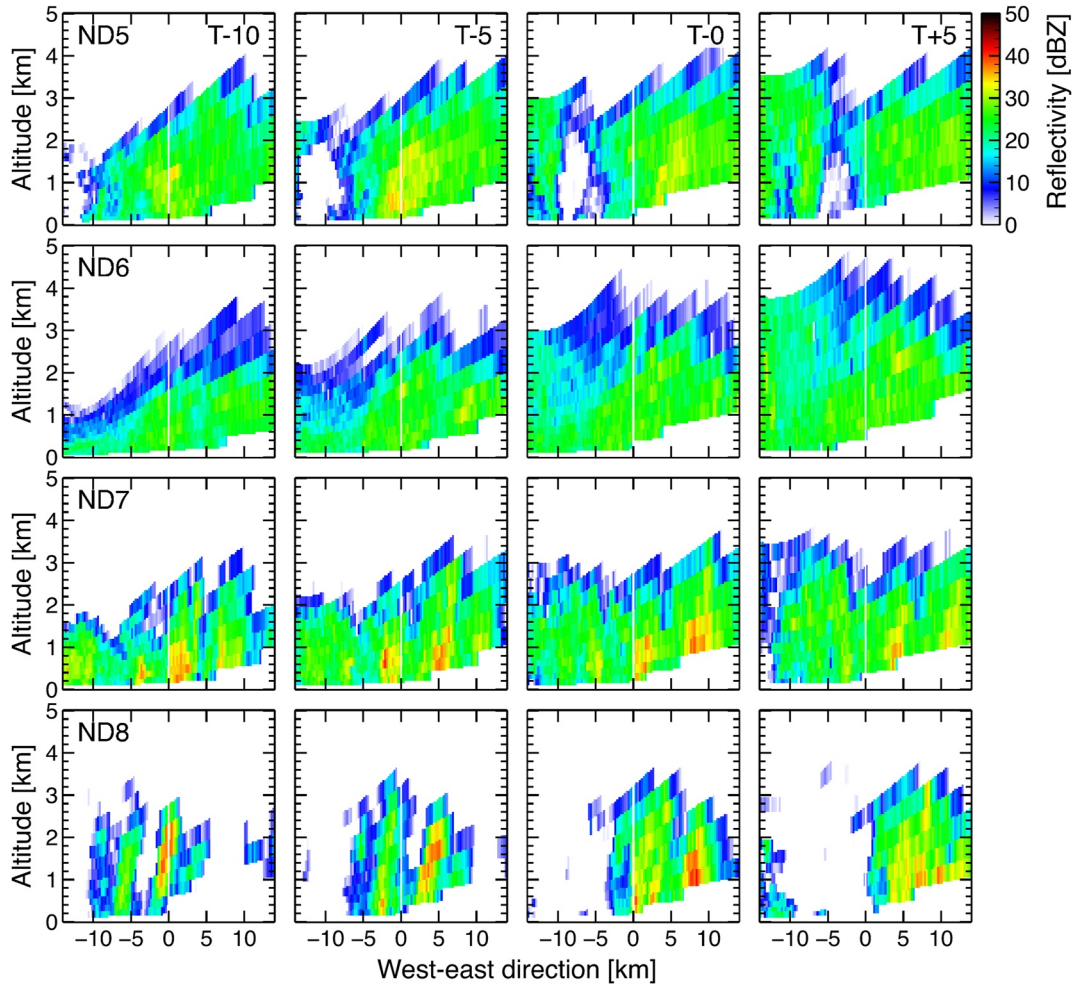

Figure 13. Time series of range-height-indicator cross-sections for the non-detection cases ND5–ND8, in the same format as Figure 11.

with convective clouds enough to produce gamma-ray glows. On the other hand, the other three non-detection cases were associated with deep convection, and were indistinguishable from the glow-detection cases, except for gamma-ray fluxes.

Data Availability Statement

The materials presented in this study are available online (Wada, 2023). The XRAIN data set can be obtained through the Data Integration and Analysis System (https://diasjp.net/en/service/xrain-original-data-download-system/) with registration. The MSM data sets of JMA can be obtained through Research Institute for Sustainable Humanosphere Data Server, Kyoto University (http://database.rish.kyoto-u.ac.jp/arch/jmadata/data/gpv/original/).

Acknowledgments
We appreciate valuable review comments from Dr. Earle Williams and two anonymous referees. The $Be_4Ge_3O_{12}$ scintillation crystal of the present study is provided by Dr. Sakurai, Dr. Niikura, and the nuclear experiment group at the University of Tokyo. The XRAIN data is provided by the Japan Ministry of Land, Infrastructure, Transport and Tourism, retrieved from Data Integration and Analysis System, The University of Tokyo. This research is supported by JSPS/MEXT KAKENHI Grants 19H00683, 21H01116, and 22K14453.

References

Bowers, G. S., Blaine, W., Shao, X.-M., Dingus, B., Smith, D. M., Schneider, M., et al. (2019). Combining Cherenkov and scintillation detector observations with simulations to deduce the nature of high-energy radiation excesses during thunderstorms. *Physical Review D*, *100*(4), 043021. https://doi.org/10.1103/physrevd.100.043021

Brook, M., Nakano, M., Krehbiel, P., & Takeuti, T. (1982). The electrical structure of the Hokuriku winter thunderstorms. *Journal of Geophysical Research*, *87*(C2), 1207–1215. https://doi.org/10.1029/jc087ic02p01207

Chilingarian, A., Daryan, A., Arakelyan, K., Hovhannisyan, A., Mailyan, B., Melkumyan, L., et al. (2010). Ground-based observations of thunderstorm-correlated fluxes of high-energy electrons, gamma rays, and neutrons. *Physical Review D*, *82*(4), 043009. https://doi.org/10.1103/physrevd.82.043009

Chilingarian, A., Hovsepyan, G., Aslanyan, D., Karapetyan, T., Khanikyanc, Y., Kozliner, L., et al. (2022). Thunderstorm ground enhancements: Multivariate analysis of 12 years of observations. *Physical Review D*, *106*(8), 082004. https://doi.org/10.1103/physrevd.106.082004

Chilingarian, A., Hovsepyan, G., & Vanyan, L. (2014). On the origin of the particle fluxes from the thunderclouds: Energy spectra analysis. *EPL*, *106*(5), 59001. https://doi.org/10.1209/0295-5075/106/59001

Chilingarian, A., Mailyan, B., & Vanyan, L. (2012). Recovering of the energy spectra of electrons and gamma rays coming from the thunderclouds. *Atmospheric Research*, *114–115*, 1–16. https://doi.org/10.1016/j.atmosres.2012.05.008

Chilingarian, A., & Mkrtchyan, H. (2012). Role of the lower positive charge region (LPCR) in initiation of the thunderstorm ground enhancements (TGES). *Physical Review D*, *86*(7), 072003. https://doi.org/10.1103/physrevd.86.072003

Chilingarian, A., Mkrtchyan, H., Karapetyan, G., Chilingaryan, S., Sargsyan, B., & Arestakesyan, A. (2019). Catalog of 2017 thunderstorm ground enhancement (TGE) events observed on Aragats. *Scientific Reports*, *9*(1), 6253. https://doi.org/10.1038/s41598-019-42786-7

Chum, J., Langer, R., Baše, J., Kollárik, M., Strhárský, I., Diendorfer, G., & Rusz, J. (2020). Significant enhancements of secondary cosmic rays and electric field at the high mountain peak of Lomnický Štít in High Tatras during thunderstorms. *Earth Planets and Space*, *72*(1), 28. https://doi.org/10.1186/s40623-020-01155-9

Cramer, E. S., Mailyan, B. G., Celestin, S., & Dwyer, J. R. (2017). A simulation study on the electric field spectral dependence of thunderstorm ground enhancements and gamma ray glows. *Journal of Geophysical Research: Atmospheres*, *122*(9), 4763–4772. https://doi.org/10.1002/2016jd026422

Diniz, G., Wada, Y., Ohira, Y., Nakazawa, K., & Enoto, T. (2022). Atmospheric electron spatial range extended by thundercloud electric field below the relativistic runaway electron avalanche threshold. *Journal of Geophysical Research: Atmospheres*, *127*(3), e2021JD035958. https://doi.org/10.1029/2021jd035958

Diniz, G. S., Wada, Y., Ohira, Y., Nakazawa, K., Tsurumi, M., & Enoto, T. (2023). Ambient conditions of winter thunderstorms in Japan to reproduce observed gamma-ray glow energy spectra. *Journal of Geophysical Research: Atmospheres*, *128*(10), e2022JD038246. https://doi.org/10.1029/2022jd038246

Dwyer, J. R. (2003). A fundamental limit on electric fields in air. *Geophysical Research Letters*, *30*(20), 2055. https://doi.org/10.1029/2003gl017781

Eack, K. B., & Beasley, W. H. (2015). Long-duration X-ray emissions observed in thunderstorms. *Journal of Geophysical Research: Atmospheres*, *120*(14), 6887–6897. https://doi.org/10.1002/2015jd023262

Eack, K. B., Beasley, W. H., Rust, W. D., Marshall, T. C., & Stolzenburg, M. (1996). Initial results from simultaneous observation of X-rays and electric fields in a thunderstorm. *Journal of Geophysical Research*, *101*(D23), 29637–29640. https://doi.org/10.1029/96jd01705

Gurevich, A., Milikh, G., & Roussel-Dupre, R. (1992). Runaway electron mechanism of air breakdown and preconditioning during a thunderstorm. *Physics Letters A*, *165*(5–6), 463–468. https://doi.org/10.1016/0375-9601(92)90348-p

Gurevich, A. V., & Zybin, K. P. (2001). Runaway breakdown and electric discharges in thunderstorms. *Physics-Uspekhi*, *44*(11), 1119–1140. https://doi.org/10.1070/pu2001v044n11abeh000939

Hisadomi, S., Nakazawa, K., Wada, Y., Tsuji, Y., Enoto, T., Shinoda, T., et al. (2021). Multiple gamma-ray glows and a downward TGF observed from nearby thunderclouds. *Journal of Geophysical Research: Atmospheres*, *126*(18), e2021JD034543. https://doi.org/10.1029/2021jd034543

Ishii, K., Hayashi, S., & Fujibe, F. (2014). Statistical analysis of temporal and spatial distributions of cloud-to-ground lightning in Japan from 2002 to 2008. *Journal of Atmospheric Electricity*, *34*(2), 79–86. https://doi.org/10.1541/jae.34.79

Japan Meteorological Agency. (2023a). Observation and statistics of lightning flashes. Retrieved from https://www.jma.go.jp/jma/kishou/know/toppuu/thunder1-1.html

Japan Meteorological Agency. (2023b). Outline of the operational numerical weather prediction at the Japan Meteorological Agency. Retrieved from https://www.jma.go.jp/jma/jma-eng/jma-center/nwp/outline2023-nwp/index.htm

Kelley, N. A., Smith, D. M., Dwyer, J. R., Splitt, M., Lazarus, S., Martinez-McKinney, F., et al. (2015). Relativistic electron avalanches as a thunderstorm discharge competing with lightning. *Nature Communications*, *6*(1), 7845. https://doi.org/10.1038/ncomms8845

Kitagawa, N. (1992). Charge distribution of winter thunderclouds. *Journal of Atmospheric Electricity*, *12*(2), 143–153. https://doi.org/10.1541/jae.12.143

Kitagawa, N., & Michimoto, K. (1994). Meteorological and electrical aspects of winter thunderclouds. *Journal of Geophysical Research*, *99*(D5), 10713. https://doi.org/10.1029/94jd00288

Kochkin, P., Sarria, D., Lehtinen, N., Mezentsev, A., Yang, S., Genov, G., et al. (2021). A rapid gamma-ray glow flux reduction observed from 20 km altitude. *Journal of Geophysical Research: Atmospheres*, *126*(9), e2020JD033467. https://doi.org/10.1029/2020jd033467

Kochkin, P., van Deursen, A. P. J., Marisaldi, M., Ursi, A., de Boer, A. I., Bardet, M., et al. (2017). In-flight observation of gamma ray glows by ILDAS. *Journal of Geophysical Research: Atmospheres*, *122*(23), 12–801. https://doi.org/10.1002/2017jd027405

Kudela, K., Chum, J., Kollárik, M., Langer, R., Strhárský, I., & Baše, J. (2017). Correlations between secondary cosmic ray rates and strong electric fields at Lomnický Štít. *Journal of Geophysical Research: Atmospheres*, *122*(20), 10700–10710. https://doi.org/10.1002/2016jd026439

Kuroda, Y., Oguri, S., Kato, Y., Nakata, R., Inoue, Y., Ito, C., & Minowa, M. (2016). Observation of gamma ray bursts at ground level under the thunderclouds. *Physics Letters B*, *758*, 286–291. https://doi.org/10.1016/j.physletb.2016.05.029

Lhermitte, R., & Williams, E. (1985). Thunderstorm electrification: A case study. *Journal of Geophysical Research*, *90*(D4), 6071–6078. https://doi.org/10.1029/jd090id04p06071

McCarthy, M., & Parks, G. K. (1985). Further observations of X-rays inside thunderstorms. *Geophysical Research Letters*, *12*(6), 393–396. https://doi.org/10.1029/gl012i006p00393

Østgaard, N., Christian, H., Grove, J., Sarria, D., Mezentsev, A., Kochkin, P., et al. (2019). Gamma-ray glow observations at 20 km altitude. *Journal of Geophysical Research: Atmospheres*. https://doi.org/10.1029/2019jd030312

Parks, G. K., Mauk, B. H., Spiger, R., & Chin, J. (1981). X-ray enhancements detected during thunderstorm and lightning activities. *Geophysical Research Letters*, *8*(11), 1176–1179. https://doi.org/10.1029/gl008i011p01176

Rakov, V. A., & Uman, M. A. (2003). *Lightning: Physics and effects*. Cambridge University Press. Retrieved from https://books.google.co.jp/books?id=TuMa5lAa3RAC

Sarria, D., Østgaard, N., Marisaldi, M., Lehtinen, N., & Mezentsev, A. (2023). Library of simulated gamma-ray glows and application to previous airborne observations. *Journal of Geophysical Research: Atmospheres*, *128*(9), e2022JD037956. https://doi.org/10.1029/2022jd037956

Saunders, C. P. R., & Peck, S. L. (1998). Laboratory studies of the influence of the rime accretion rate on charge transfer during crystal/graupel collisions. *Journal of Geophysical Research*, *103*(D12), 13949–13956. https://doi.org/10.1029/97jd02644

Takahashi, T., Sugimoto, S., Kawano, T., & Suzuki, K. (2017). Riming electrification in Hokuriku winter clouds and comparison with laboratory observations. *Journal of the Atmospheric Sciences*, *74*(2), 431–447. https://doi.org/10.1175/JAS-D-16-0154.1

Takahashi, T., Sugimoto, S., Kawano, T., & Suzuki, K. (2019). Microphysical structure and lightning initiation in Hokuriku winter clouds. *Journal of Geophysical Research: Atmospheres*, *124*(23), 13156–13181. https://doi.org/10.1029/2018jd030227

Takahashi, T., Tajiri, T., & Sonoi, Y. (1999). Charges on graupel and snow crystals and the electrical structure of winter thunderstorms. *Journal of the Atmospheric Sciences*, *56*(11), 1561–1578. https://doi.org/10.1175/1520-0469(1999)056⟨1561:cogasc⟩2.0.co;2

Takeuti, T., Nakano, M., Brook, M., Raymond, D. J., & Krehbiel, P. (1978). The anomalous winter thunderstorms of the Hokuriku coast. *Journal of Geophysical Research*, *83*(C5), 2385–2394. https://doi.org/10.1029/jc083ic05p02385

Torii, T., Sugita, T., Tanabe, S., Kimura, Y., Kamogawa, M., Yajima, K., & Yasuda, H. (2009). Gradual increase of energetic radiation associated with thunderstorm activity at the top of Mt. Fuji. *Geophysical Research Letters*, *36*(13), L13804. https://doi.org/10.1029/2008gl037105

Torii, T., Takeishi, M., & Hosono, T. (2002). Observation of gamma-ray dose increase associated with winter thunderstorm and lightning activity. *Journal of Geophysical Research*, *107*(D17), ACL 2–1–ACL 2–13. https://doi.org/10.1029/2001jd000938

Tsuchiya, H., Enoto, T., Iwata, K., Yamada, S., Yuasa, T., Kitaguchi, T., et al. (2013). Hardening and termination of long-duration γ rays detected prior to lightning. *Physical Review Letters*, *111*(1), 015001. https://doi.org/10.1103/physrevlett.111.015001

Tsuchiya, H., Enoto, T., Torii, T., Nakazawa, K., Yuasa, T., Torii, S., et al. (2009). Observation of an energetic radiation burst from mountain-top thunderclouds. *Physical Review Letters*, *102*(25), 255003. https://doi.org/10.1103/physrevlett.102.255003

Tsuchiya, H., Enoto, T., Yamada, S., Yuasa, T., Kawaharada, M., Kitaguchi, T., et al. (2007). Detection of high-energy gamma rays from winter thunderclouds. *Physical Review Letters*, *99*(16), 165002. https://doi.org/10.1103/physrevlett.99.165002

Tsuchiya, H., Enoto, T., Yamada, S., Yuasa, T., Nakazawa, K., Kitaguchi, T., et al. (2011). Long-duration γ ray emissions from 2007 and 2008 winter thunderstorms. *Journal of Geophysical Research*, *116*(D9), D09113. https://doi.org/10.1029/2010jd015161

Tsuchiya, H., Hibino, K., Kawata, K., Hotta, N., Tateyama, N., Ohnishi, M., et al. (2012). Observation of thundercloud-related gamma rays and neutrons in Tibet. *Physical Review D*, *85*(9), 092006. https://doi.org/10.1103/physrevd.85.092006

Wada, Y. (2023). Materials for "Negative excursion of surface electric fields during gamma-ray glows in winter thunderstorms" [Dataset]. Mendeley. https://doi.org/10.17632/4kbryzxwbk.1

Wada, Y., Bowers, G. S., Enoto, T., Kamogawa, M., Nakamura, Y., Morimoto, T., et al. (2018). Termination of electron acceleration in thundercloud by intracloud/intercloud discharge. *Geophysical Research Letters*, *45*(11), 5700–5707. https://doi.org/10.1029/2018gl077784

Wada, Y., Enoto, T., Kubo, M., Nakazawa, K., Shinoda, T., Yonetoku, D., et al. (2021). Meteorological aspects of gamma-ray glows in winter thunderstorms. *Geophysical Research Letters*, *48*(7), e2020GL091910. https://doi.org/10.1029/2020gl091910

Wada, Y., Enoto, T., Nakamura, Y., Furuta, Y., Yuasa, T., Nakazawa, K., et al. (2019). Gamma-ray glow preceding downward terrestrial gamma-ray flash. *Communications Physics*, *2*(1), 67. https://doi.org/10.1038/s42005-019-0168-y

Wada, Y., Matsumoto, T., Enoto, T., Nakazawa, K., Yuasa, T., Furuta, Y., et al. (2021). Catalog of gamma-ray glows during four winter seasons in Japan. *Physical Review Research*, *3*(4), 043117. https://doi.org/10.1103/physrevresearch.3.043117

Wada, Y., Tsurumi, M., Hayashi, S., & Michimoto, K. (2023). Synoptic meteorological conditions of gamma-ray glows in winter thunderstorms. *Progress in Earth and Planetary Science*, *10*(1), 6. https://doi.org/10.1186/s40645-023-00538-2

Wada, Y., Wu, T., Wang, D., Enoto, T., Nakazawa, K., Morimoto, T., et al. (2023). Termination of downward-oriented gamma-ray glow by normal-polarity in-cloud discharge activity. *Journal of Geophysical Research: Atmospheres*, *128*(15), e2023JD038606. https://doi.org/10.1029/2023jd038606

Williams, E. (2018). Lightning activity in winter storms: A meteorological and cloud microphysical perspective. *IEEJ Transactions on Power and Energy*, *138*(5), 364–373. https://doi.org/10.1541/ieejpes.138.364

Williams, E., Mkrtchyan, H., Mailyan, B., Karapetyan, G., & Hovakimyan, S. (2022). Radar diagnosis of the thundercloud electron accelerator. *Journal of Geophysical Research: Atmospheres*, *127*(11), e2021JD035957. https://doi.org/10.1029/2021jd035957

Williams, E. R. (1989). The tripole structure of thunderstorms. *Journal of Geophysical Research*, *94*(D11), 13151–13167. https://doi.org/10.1029/jd094id11p13151

Wilson, C. T. R. (1925). The acceleration of β-particles in strong electric fields such as those of thunderclouds. *Mathematical Proceedings of the Cambridge Philosophical Society*, *22*(04), 534–538. https://doi.org/10.1017/s0305004100003236

Yoshida, S., Yoshikawa, E., Adachi, T., Kusunoki, K., Hayashi, S., & Inoue, H. (2018). Three-dimensional radio images of winter lightning in Japan and characteristics of associated charge structure. *IEEJ Transactions on Electrical and Electronic Engineering*, *14*(2), 175–184. https://doi.org/10.1002/tee.22795

Yuasa, T., Wada, Y., Enoto, T., Furuta, Y., Tsuchiya, H., Hisadomi, S., et al. (2020). Thundercloud project: Exploring high-energy phenomena in thundercloud and lightning. *Progress of Theoretical and Experimental Physics*, *2020*(10), 103H01. https://doi.org/10.1093/ptep/ptaa115

Zhang, Z.-B., & Choi, C.-S. (2008). An analysis of the durations of swift gamma-ray bursts. *Astronomy and Astrophysics*, *484*(2), 293–297. https://doi.org/10.1051/0004-6361:20079210

Zheng, D., Wang, D., Zhang, Y., Wu, T., & Takagi, N. (2019). Charge regions indicated by LMA lightning flashes in Hokuriku's winter thunderstorms. *Journal of Geophysical Research: Atmospheres*, *124*(13), 7179–7206. https://doi.org/10.1029/2018jd030060